AERODYNAMIC CHARACTERISTICS FROM WIND-TUNNEL STUDIES OF THE X-15 CONFIGURATION

By Herbert W. Ridyard and Robert W. Dunning
Langley Aeronautical Laboratory

and E. W. Johnston
North American Aviation, Inc.

INTRODUCTION

In order to investigate the aerodynamic characteristics of the X-15 research airplane, an exploratory wind-tunnel test program was initiated in January of 1956. Since that time, X-15 models have been tested in eight different facilities through a Mach number range from less than 0.1 to about 6.9. Several variations of the original configuration have been tested. The aerodynamic characteristics of two of the configurations are presented in this paper.

DISCUSSION

A three-view sketch of these two configurations with speed brakes deflected 45° is shown in figure 1. Some of the differences between the two configurations are indicated by the solid and dashed lines. Configuration 1, which is indicated by the solid lines, represents the original proposed design by the North American Aviation, Inc. (See ref. 1 for description.) Configuration 2, as indicated by the dashed lines, is a revised configuration and is the configuration described in the preceding paper by Charles H. Feltz and in reference 2.

The primary difference between the configurations is that the nose of configuration 2 is considerably more blunt than that of configuration 1. This increase in bluntness was necessary to provide an increase in fuel capacity. The diameter of the basic body of revolution was increased about 6 percent for the same reason. The wing was moved rearward about 2.5 percent of the mean aerodynamic chord in an attempt to balance aerodynamically the change in nose shape. It should be noted that the center of gravity was moved also so that it would be located at 25 percent of the mean aerodynamic chord for either configuration.

In addition to these differences, the rear portions of the side fairings were enlarged for configuration 2 as shown in figure 1. The landing skids (shown in the retracted position in fig. 1) were moved rearward from beneath the wing on configuration 1 to a position beneath

the horizontal tail. Finally, the leading-edge radii of the wing and tail surfaces and the radius at the tip of the body nose were increased to satisfy the aerodynamic-heating requirements.

Figure 2 presents the wind-tunnel program for these two configurations. The facilities utilized in this program are the North American 8.75- by 11-foot tunnel, the Langley 8-foot transonic tunnel, the North American 16-inch tunnel, the Massachusetts Institute of Technology supersonic tunnel, the Langley 9- by 9-inch Mach number 4 blowdown jet, the Ames 10- × 14-inch tunnel, and the Langley 11-inch hypersonic tunnel. The data presented in this paper are unpublished preliminary results obtained from these facilities. The test Mach number range is illustrated by the bar graph at the right of figure 2. Note that configuration 1 has been tested in each facility whereas configuration 2 has been tested only in three facilities.

The drag characteristics of the X-15 are shown in figure 3. This figure presents the effect of speed-brake deflection on the drag coefficient at an angle of attack of 0° over the test Mach number range. The results presented in this figure are for brakes closed and deflected 20°, 30°, and 45°. Note that the open symbols refer to configuration 1 and the shaded symbols to configuration 2. This method of identification of the results for the two configurations will be used throughout the paper.

As noted in the previous paper by Feltz, the drag of the configuration with the speed brakes closed is not of major importance in the design performance of the airplane. For the configurations with the speed brakes deflected, high values of drag coefficient are important for speed control during reentry, and these high values are seen to be available; in fact, the values presented in figure 3 for the speed brake deflected 45° are so high that the speed brakes require a blow-back feature such as that discussed by Charles H. Feltz.

Another point of interest is that the variation of drag coefficient with speed-brake deflection is considerably more nonlinear at a Mach number of 6.86 than at a Mach number of 3 or 4.

The effect of lift coefficient on drag coefficient is shown in figure 4. These results are for Mach numbers of 1.43 and 6.86 and for configuration 1 with speed brakes closed and deflected 45°. It is apparent from figure 4 that the drag due to lift increases greatly with Mach number; however, even for the higher Mach number, in order to obtain the same drag coefficient, it is necessary to go to a much higher lift coefficient with the speed brakes closed than with speed brakes deflected to 45°.

Figure 5 presents the variation of lift-curve slope at an angle of attack of 0° with Mach number. These data, as indicated by the front-view sketches, are for the following configurations: the complete airplane; the body, wing, and side fairing; the body and side fairing; and the basic body of revolution. It is shown that the lift-curve slopes for the complete and the body-wing configurations decrease with Mach number in the supersonic speed range. This decrease is primarily due to the loss in lifting effectiveness of the wing. On the other hand, for the body configurations the lift-curve slope remains relatively constant with Mach number. The end result is that at a Mach number of 6.86 almost one-half of the total lift of the complete airplane is derived from the body—side-fairing configuration. Further inspection of figure 5 indicates that about one-fourth of the lift of the airplane is derived from the side fairings at this same Mach number (6.86). Although not shown in figure 5, speed-brake deflection had little effect on the lift-curve slope of the complete airplane throughout the Mach number range.

Figure 6 presents the variation of lift coefficient with angle of attack for configuration 1 at several Mach numbers. The data show that nonlinearities are small up to a Mach number of 3; however, at a Mach number of 6.86 the curve is somewhat nonlinear. Although it is not readily apparent from figure 6, the value of C_L at $\alpha = 20°$, obtained by extrapolation by use of the lift-curve slope at an angle of attack of 0°, is about 50 percent lower than the experimental value of C_L at $\alpha = 20°$. Attempts to estimate the data for a Mach number of 6.86 have not been entirely successful up to the present time, primarily because of the nonsymmetrical cross section of the fuselage. However, estimates obtained by a summation of experimental lift coefficients for the body and theoretical coefficients for the wing and tail surfaces, calculated by use of shock-expansion theory, are in excellent agreement with the data at a Mach number of 6.86.

Figure 7 depicts the variation of the longitudinal-stability parameter dC_m/dC_L at $C_L = 0$ with Mach number for the following configurations: the body and side fairing; the body, wing, and side fairing; and the complete airplane. The data for configuration 1 (open symbols) show that the configuration of body and side fairing is unstable throughout the Mach number range; however, this instability decreases with Mach number because of a rearward movement of the center of pressure. The configuration of body, wing, and side fairing, which is unstable at subsonic Mach numbers, the center of gravity being located at one-quarter of the mean aerodynamic chord, becomes stable at low supersonic Mach numbers as the wing center of pressure moves rearward. This configuration then decreases in stability at higher Mach numbers as the wing effectiveness decreases.

The complete configuration 1 is stable throughout the Mach number range as a result of the large tail input; however, there are two regions of marginal stability, one at subsonic speeds and one at hypersonic speeds. As a matter of fact, there is a dip to almost neutral stability at a Mach number of 0.95. These regions of marginal stability are restricted to small lift coefficients as is shown in figure 8 which presents the variation of the pitching-moment coefficient with lift coefficient for configuration 1 with the speed brakes closed for several Mach numbers. The results for configuration 2 are also included for comparison in figure 8 for a Mach number of 6.86. For configuration 1 the longitudinal stability is marginal at small values of lift coefficient for Mach numbers of 0.95 and 6.86; however, the slopes of these curves at high values of lift coefficient are nearly as great as that for a Mach number of 1.43. Therefore, the problem of longitudinal stability is not as serious for high values of lift coefficients as for low values of lift coefficient.

The longitudinal stability of configuration 2 is indicated by the shaded symbols in figures 7 and 8. It is obvious that all the results for zero-lift coefficient show less stability at supersonic Mach numbers. At a Mach number of 6.86 the complete configuration is shown to be unstable, the center of gravity being located at one-quarter of the mean aerodynamic chord. This decrease in stability can apparently be traced to the increased bluntness of the fuselage of configuration 2 as shown by the shift in all three sets of data points at a Mach number of 6.86 in the destabilizing direction. (See fig. 7.)

As a possible means of improving the longitudinal stability of the complete configuration, the body and side fairing of configuration 1 was modified by removing part of the side fairing in the vicinity of the nose. Additional tests (not presented herein) obtained with this modified configuration in the Langley 11-inch hypersonic tunnel have indicated large gains in stability. It is therefore plausible to assume that a similar removal of the side fairing from configuration 2 would restore a large part of this decrease in stability. Further considerations of possible means of improving the longitudinal stability are discussed in a subsequent paper by Lawrence P. Greene.

Figure 9 presents the effect of speed-brake deflection on the longitudinal stability at zero-lift coefficient. The experimental results are for complete configurations 1 and 2 with speed brakes closed or deflected 45° as indicated by the sketches of the vertical-tail sections. It is evident that the longitudinal stability increases with speed-brake deflection, and in the higher Mach number range the stability due to the speed brakes increases greatly with Mach number.

The explanation for this effect at a particular Mach number can probably be found by considering the variations with angle of attack of the dynamic pressure in the flow fields above and below the airplane. The effect of these variations in dynamic pressure with angle of attack is to decrease the pitching-moment contribution of the upper speed brake and to increase the pitching-moment contribution of the lower speed brake; the net effect of both speed brakes is to increase the stability of the airplane. At the higher Mach numbers these variations in dynamic pressure with angle of attack are known to become more pronounced; therefore, the speed-brake effect on stability increases greatly with Mach number in the hypersonic Mach number range.

Another means of increasing the longitudinal stability of the complete configuration at high Mach numbers is described in figure 10 where the effect of horizontal-tail section on the longitudinal stability of configuration 2 is given. Pitching-moment coefficient is plotted against lift coefficient for the complete configuration with an NACA 66-series modified symmetrical horizontal-tail section and for the complete configuration with a 10° wedge horizontal-tail section. These results are compared for Mach numbers of 1.51, 3.50, and 6.86. At a Mach number of 1.51, there is no effect on the stability due to airfoil section; however, at the higher Mach numbers, the stability is greater for the wedge section. This result is particularly apparent at a Mach number of 6.86 at small values of lift coefficient where, in fact, an increase in stability is very much needed.

This increase in stability at small values of lift coefficient for a Mach number of 6.86 could have been obtained with a speed-brake deflection of about 30°; however, a higher drag penalty would have been incurred. For example, the minimum drag for the complete configuration would double with the use of a 30° speed-brake deflection; whereas the minimum drag would increase by only 10 percent with the use of a 10° wedge horizontal-tail section.

The longitudinal-control results for configuration 2 are given in figure 11. Shown in this figure are the variations in pitching-moment coefficient with lift coefficient for several horizontal-tail deflections for Mach numbers of 2 and 6.86. At a Mach number of 2 the increment in pitching moment between tail deflections is relatively constant; however, at a Mach number of 6.86, at small negative values of lift coefficient, longitudinal control is very small compared with the control at high lift coefficients.

The reason for the loss in control in the region of small negative lift coefficients is apparent in figure 12. The effect of the wing on the incremental pitching moment of the horizontal tail due to a tail deflection of -20° is shown in figure 12. These results are plotted for wing on and off through the test angle-of-attack range. At small, particularly negative, angles of attack there is a large effect of the wing

on the horizontal-tail pitching moment as indicated by the sketch at the left of the figure where the tail is deflected into the wing wake. At high angles of attack there is little effect of the wing on the horizontal-tail pitching moment since the low-dynamic-pressure flow from the wing passes over the tail as indicated by the sketch at the right.

Figure 13 presents the effect of speed-brake deflection on the longitudinal control of configuration 2 at a Mach number of 6.86. Pitching moment is plotted against lift coefficient for horizontal-tail deflections of 0°, -10°, and -20° for three speed-brake deflections. The first is a combination of deflections, 5° for the upper speed brakes and 7.5° for the lower speed brakes. These deflections transform the basic double-wedge section of the vertical tails into a single-wedge airfoil section. The other two speed-brake deflections are 20° and 45°.

All three sets of results in figure 13 show less control power at small lift coefficients than for high lift coefficients as shown in figure 12. Furthermore, there are only small differences in longitudinal control between the full-wedge speed-brake-deflection results and the 20° speed-brake-deflection results; however, for the 45° case the conditions for trim are considerably different and should be taken into account in dynamic studies of the configuration.

Since the horizontal tail provides lateral as well as longitudinal control, it is appropriate to consider the lateral-control results in figure 14. The rolling-moment and yawing-moment coefficients per degree of differential tail deflection $C_{l_{\delta_h}}$ and $C_{n_{\delta_h}}$ are plotted against Mach number. These data were obtained for the complete configuration with a differential tail deflection of $\pm 5^\circ$ and are presented for angles of attack of 0°, 10°, and 20°. As noted, some of the data are for the single-wedge vertical-tail section indicated by the 5°, 7.5° combination of speed-brake deflections and some, for the 20° speed-brake deflection.

The rolling-moment-parameter data show that, for an angle of attack of 0°, lateral control decreases with Mach number at supersonic speeds. At the higher Mach numbers, lateral control increases with angle of attack. These trends are similar to those discussed for the longitudinal-control results (fig. 11), as might have been expected.

In figure 14 $C_{n_{\delta_h}}$ is seen to decrease with Mach number, but in the higher Mach number range this parameter does not vary greatly with angle of attack.

It should be noted that the coupling parameter $C_{n_{\delta_h}}$, as defined herein, represents a favorable yawing moment; that is, the airplane will tend to yaw in the direction that it is being rolled.

Figure 15 gives the variation with Mach number of the static directional stability derivative C_{n_β} at an angle of attack of 0° for the complete configuration with speed brakes closed and deflected, as indicated by the sketches of the vertical-tail sections, and also for the vertical-tail-off configuration.

These results show that, for the speed-brakes-closed configuration, static directional stability decreases with Mach number and becomes unstable at Mach numbers above about 4.3. This loss in stability is due to the decrease in effectiveness of the double-wedge section as the Mach number is increased. The use of a full-wedge vertical section (that is, $\delta_b = 5^\circ, 7.5^\circ$) provides about neutral stability at the higher Mach numbers. The use of 45° speed brakes, however, provides large values of directional stability throughout the Mach number range.

In figure 16 is a similar presentation for the effective-dihedral parameter C_{l_β} at an angle of attack of 0°. The results for the complete configuration with speed brakes closed show that C_{l_β} decreases with Mach number. These results also show that C_{l_β} increases with speed-brake deflection in much the same way as C_{n_β}, but it should be remembered that these large negative values of C_{l_β} are primarily due to the lack of symmetry of the vertical tail.

Figure 17 presents the variation of C_{n_β} and C_{l_β} with angle of attack for configuration 2 with speed brakes deflected 20° at Mach numbers of 2.98 and 6.86. As indicated by the sketches, these results are for the complete airplane with both vertical tails, with the upper vertical tail off, and with both vertical tails off.

At a Mach number of 2.98 the directional-stability derivative C_{n_β} decreases to zero at an angle of attack of about 20° whereas for a Mach number of 6.86 C_{n_β} is fairly constant with α. At both Mach numbers the upper vertical tail loses its effectiveness with angle of attack as shown by the decrease in the increment between the curves, for the configuration with both vertical tails on and with the upper vertical tail off; whereas the lower vertical tail increases in effectiveness as shown by the increment between the curves for the configuration with the upper vertical tail off and with both vertical tails off. The main difference between the results is that at a Mach number of 6.86 the lower vertical tail increases its effectiveness by several times and thus maintains positive values of C_{n_β} at high angles of attack which are about as high as those for an angle of attack of 0°.

Although these results are only for a speed-brake deflection of 20°, they are representative of the trends for other speed-brake deflections; for example, at a Mach number of 2.98 for a smaller speed-brake deflection than 20°, the C_{n_β} curve would drop to zero at a smaller angle of attack; likewise, for a larger speed-brake angle C_{n_β} would go to zero at a higher angle of attack. For a Mach number of 6.86 the curve for the complete airplane also would shift roughly parallel to itself for other speed-brake deflections and would become more stable as the speed-brake deflection increased.

It is significant to note from these results that, if the speed brakes are used for improving directional stability, the directional-stability problem could be more critical at a Mach number of 2.98.

In figure 17 C_{l_β} for the complete airplane is seen to increase with angle of attack at a Mach number of 2.98 and to decrease with angle of attack at a Mach number of 6.86. At an angle of attack of 0° the rolling moments are negative at both Mach numbers because they are derived primarily from the upper vertical tail. At high angles of attack, at a Mach number of 2.98, C_{l_β} for the configuration with both tails off agrees closely with C_{l_β} for the complete airplane; thus, the upper and lower tail contributions to the rolling moments have about canceled each other. At high angles of attack for a Mach number of 6.86, however, C_{l_β} is less negative than the value for the configuration with both vertical tails off because the difference in rolling moments are primarily due to the lower vertical tail.

Figure 18 depicts the directional-control results for configuration 2 throughout the Mach number range. The parameters are the yawing- and rolling-moment coefficients per degree of vertical-tail deflection. These results show that, for either the full-wedge vertical tail or the 20° speed-brake deflection at an angle of attack of 0° or 20°, $C_{n_{\delta_v}}$ and $C_{l_{\delta_v}}$ decrease with Mach number and also with angle of attack. At high Mach numbers and angles of attack these parameters are approaching zero. Note that only the upper tail is movable and therefore this decrease in directional control could have been anticipated from the discussion of directional stability (fig. 17). As is discussed further by Lawrence P. Greene in a subsequent paper, the lower vertical tail will be movable on future configurations so that a considerable amount of the loss in control with angle of attack will be restored.

Finally, it is interesting to note that the magnitude of the coupling parameter $C_{l_{\delta_v}}$ at a Mach number of 6.86 is higher for an angle of attack of 0° where, as noted in figure 14, the roll-control parameter $C_{l_{\delta_h}}$ is at its lowest.

REFERENCES

1. Johnston, E. W.: Test and Model Information for Wind Tunnel Tests of a Full Span .02-Scale Weapon System 447L (X-15 Research Airplane, NA-240) Sting Mounted Force Model at the Langley 11" Hypersonic and 9" Supersonic Blowdown Jet Wind Tunnels. Rep. No. NA-56-170, North American Aviation, Inc., Feb. 8, 1956.

2. Winfrey, J. T.: Test and Model Information for Wind Tunnel Tests of a Revised Full Span .02-Scale Weapon System 447L (X-15 Research Airplane, NA-240) Sting Mounted Force Model at the Langley 11" Hypersonic and 9" Supersonic Blowdown Jet Wind Tunnels. Rep. No. NA-56-694, North American Aviation, Inc., May 31, 1956.

X-15

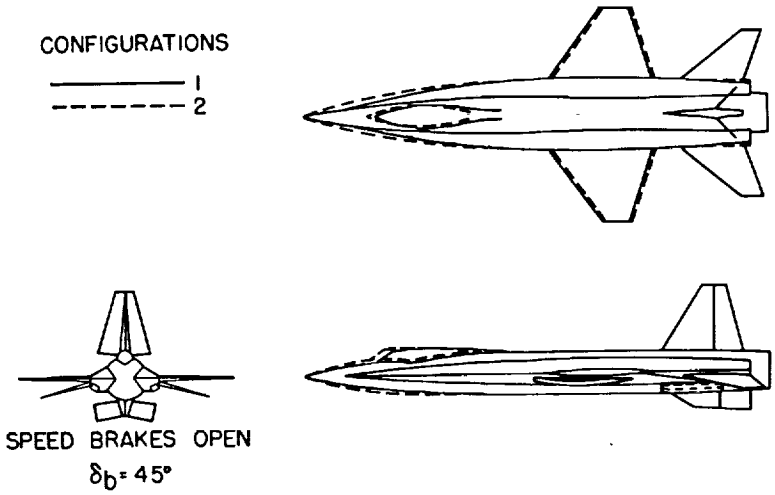

Figure 1

WIND-TUNNEL PROGRAM

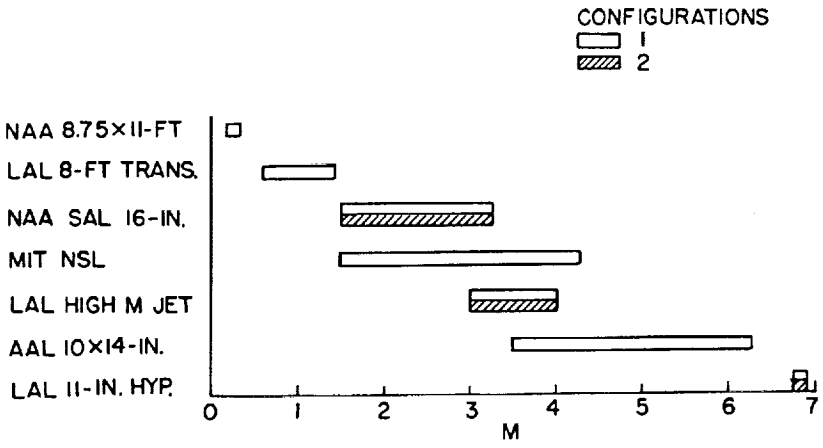

Figure 2

EFFECT OF SPEED-BRAKE DEFLECTION
ON C_D AT $\alpha = 0°$

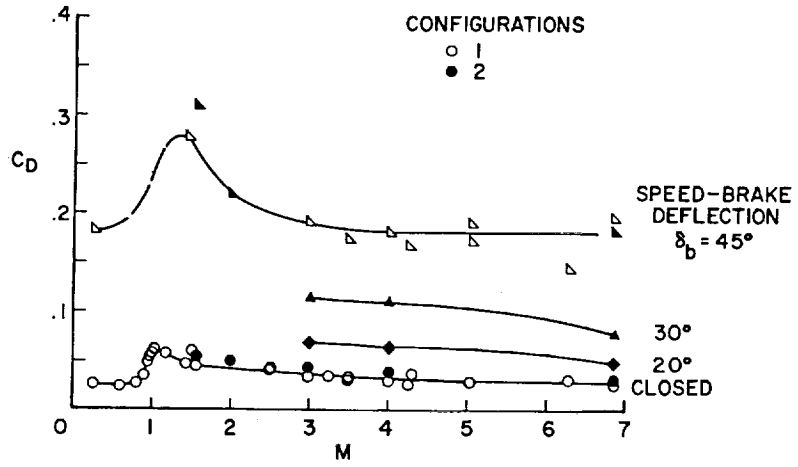

Figure 3

EFFECT OF C_L ON C_D
CONFIGURATION 1

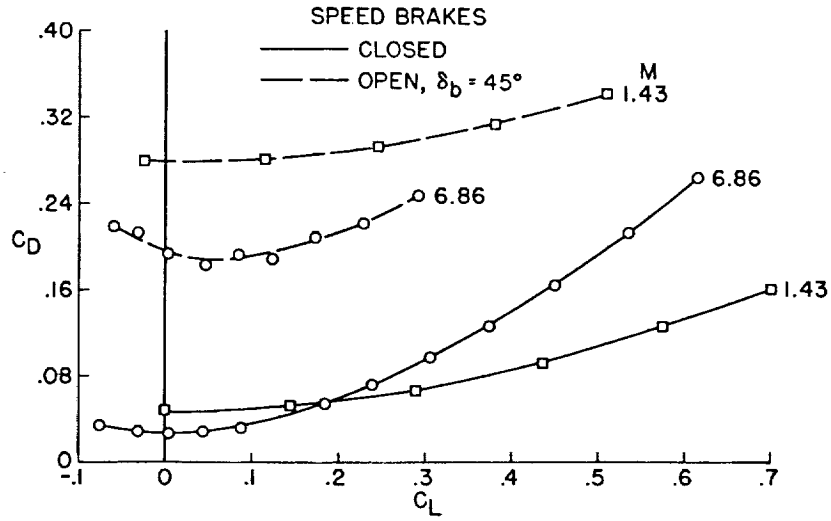

Figure 4

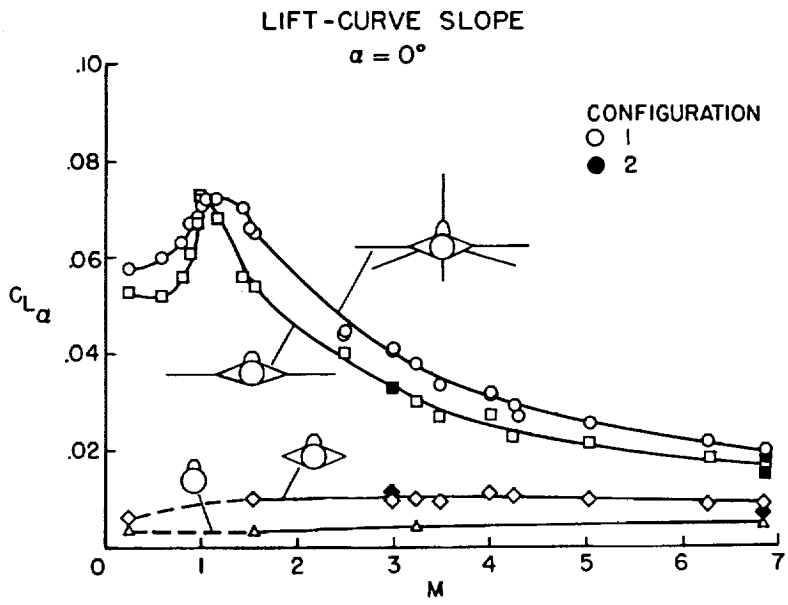

Figure 5

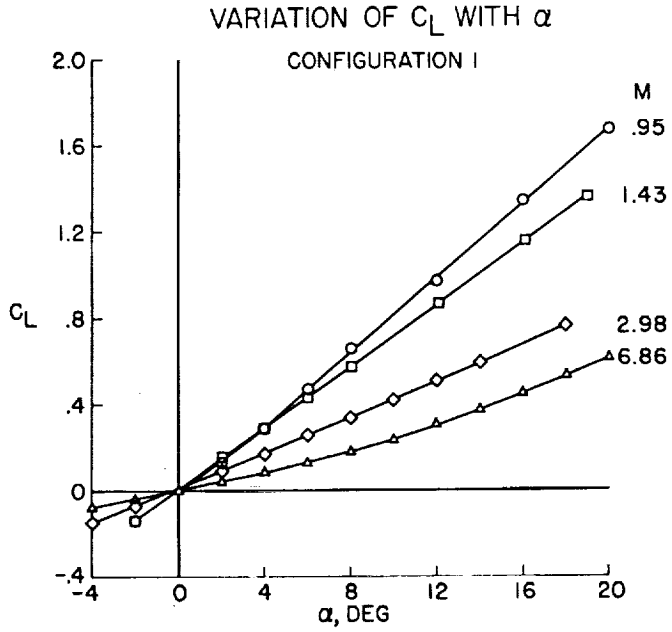

Figure 6

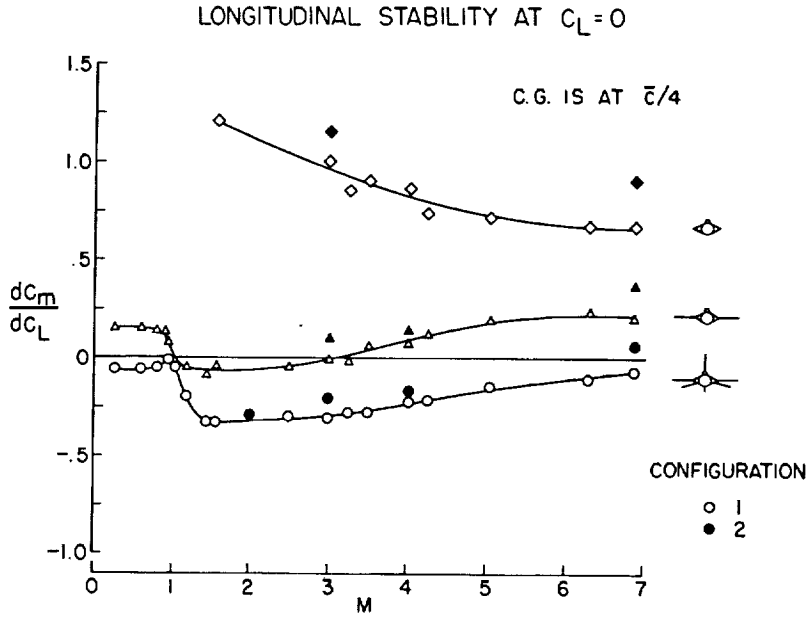

Figure 7

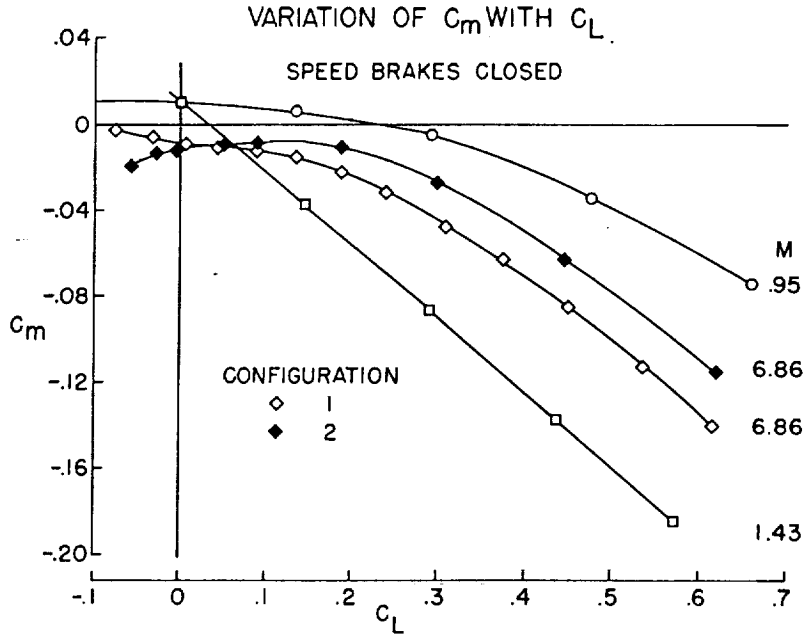

Figure 8

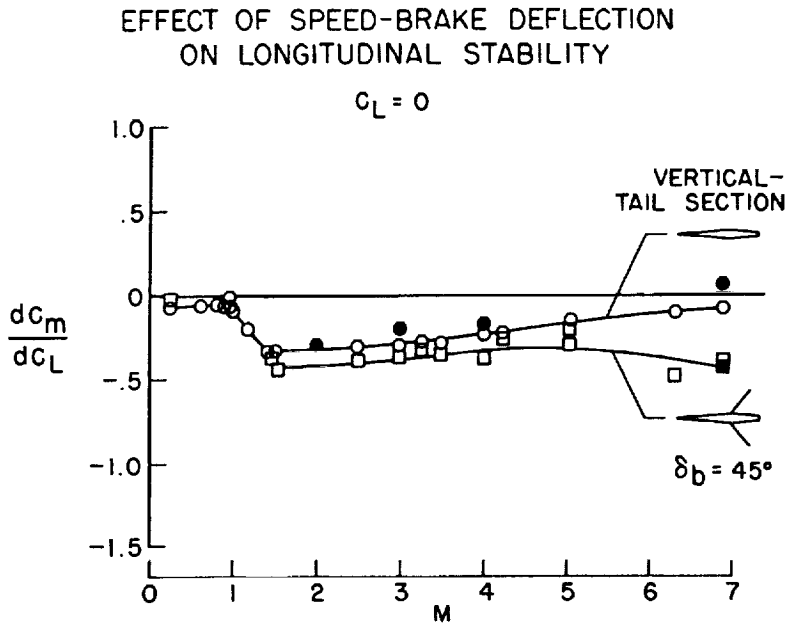

Figure 9

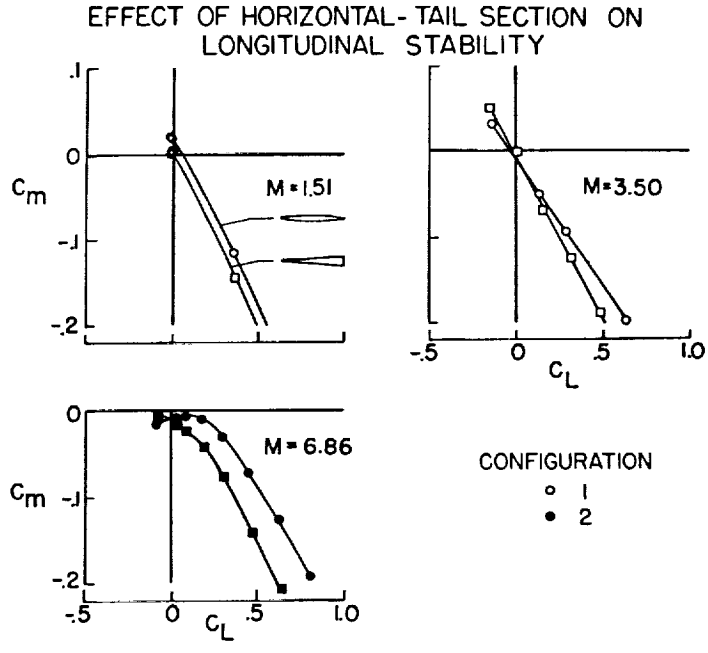

Figure 10

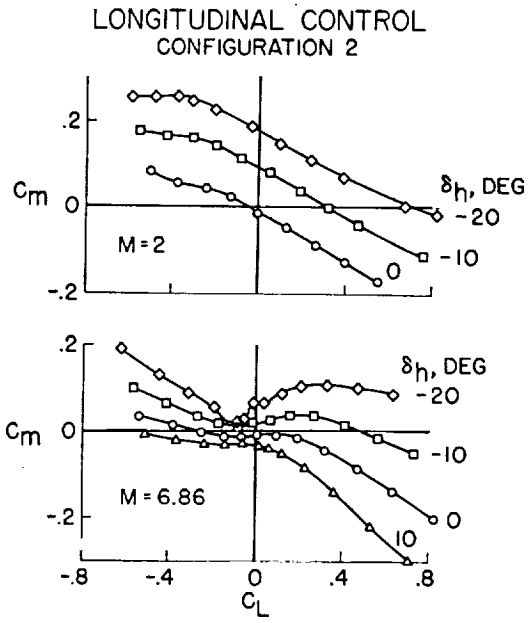

Figure 11

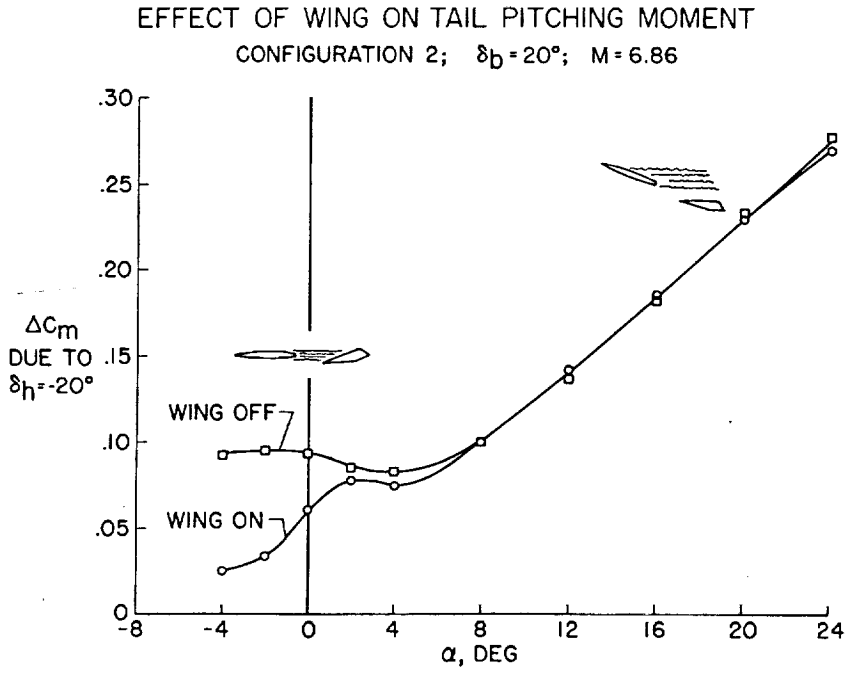

Figure 12

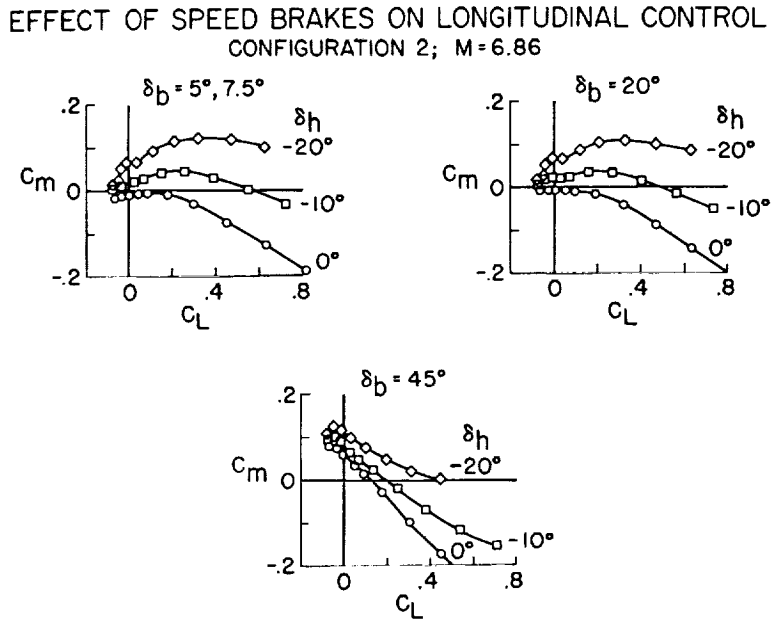

Figure 13

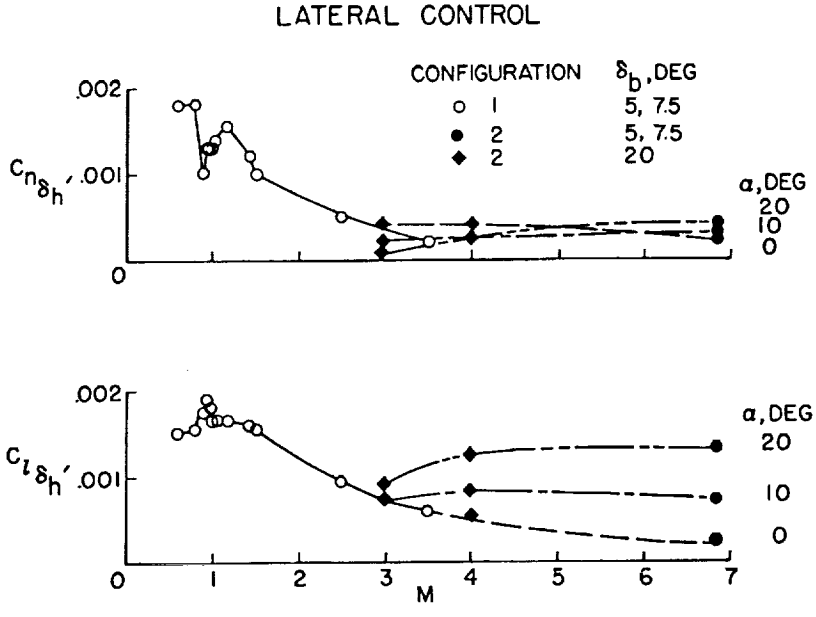

Figure 14

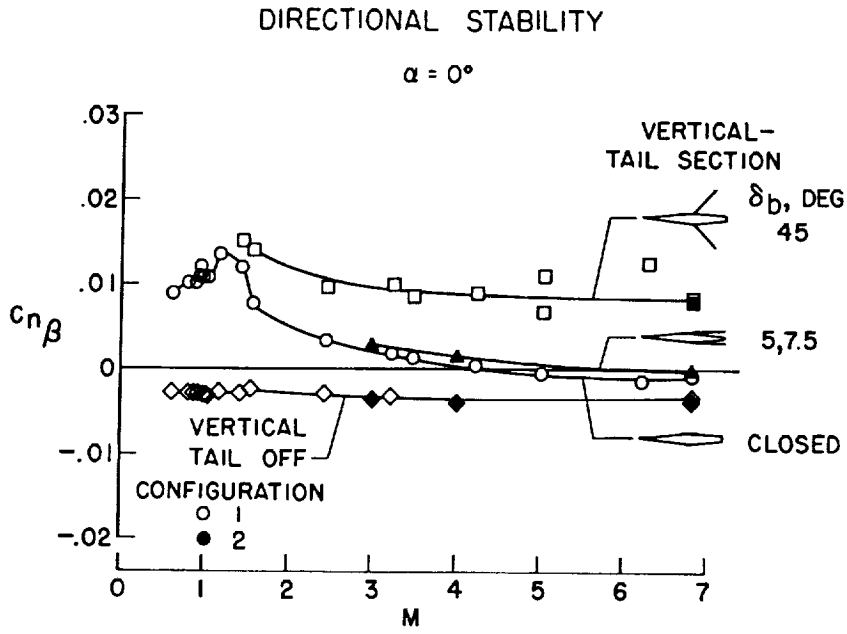

Figure 15

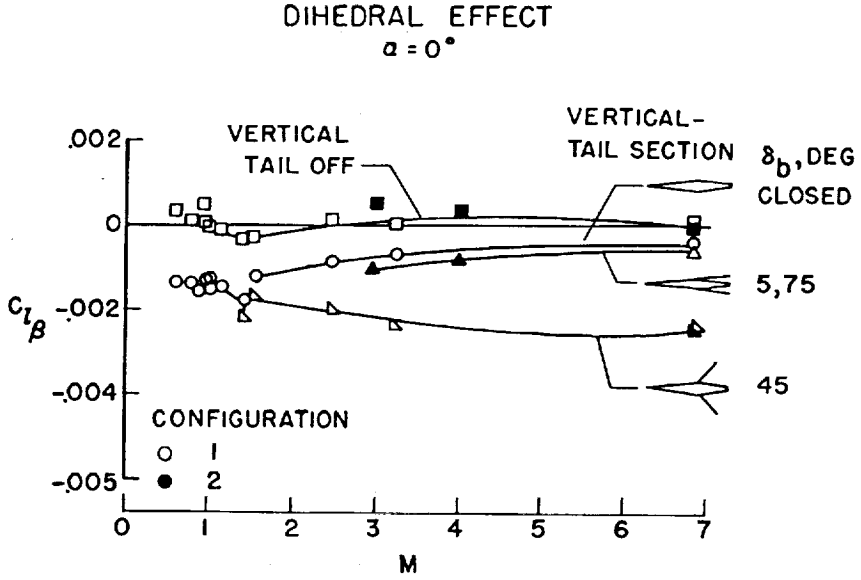

Figure 16

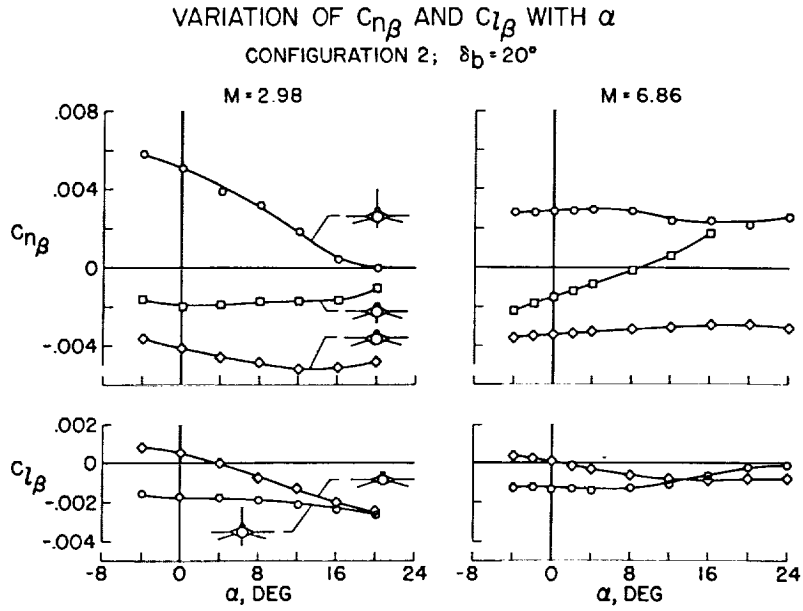

Figure 17

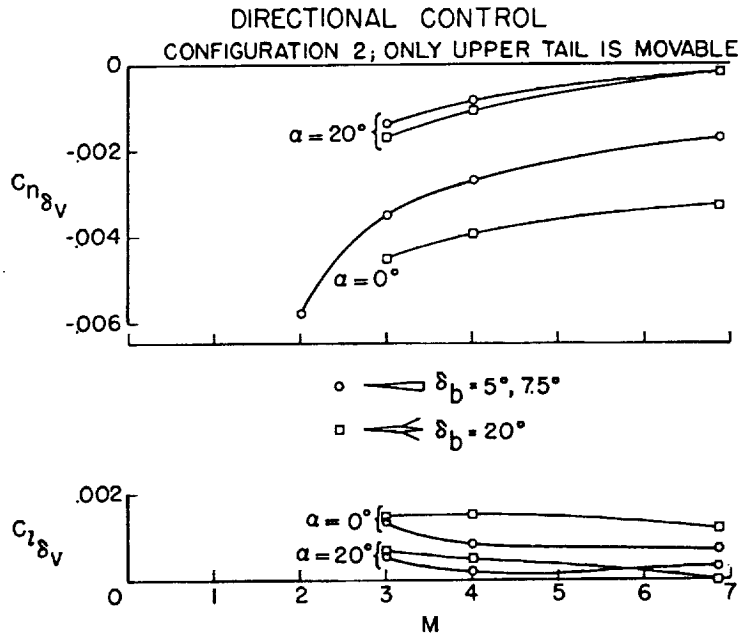

Figure 18